Representative results of two independent experiments with similar findings are shown.

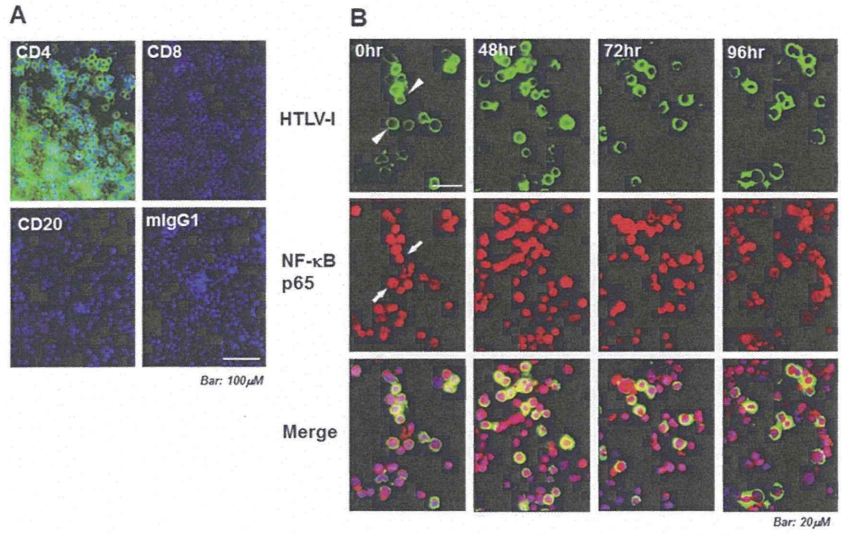

38x24mm (600 x 600 DPI)

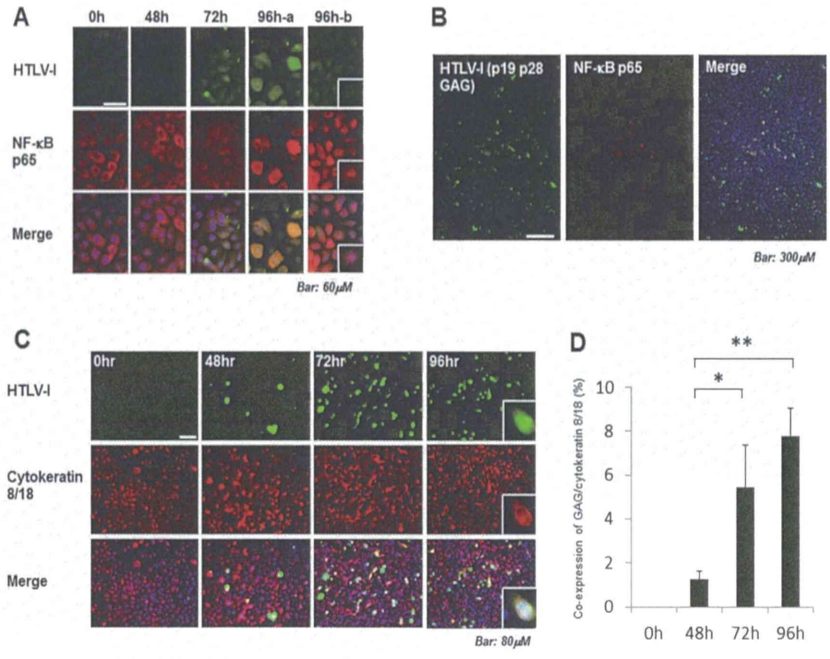

66x48mm (600 x 600 DPI)

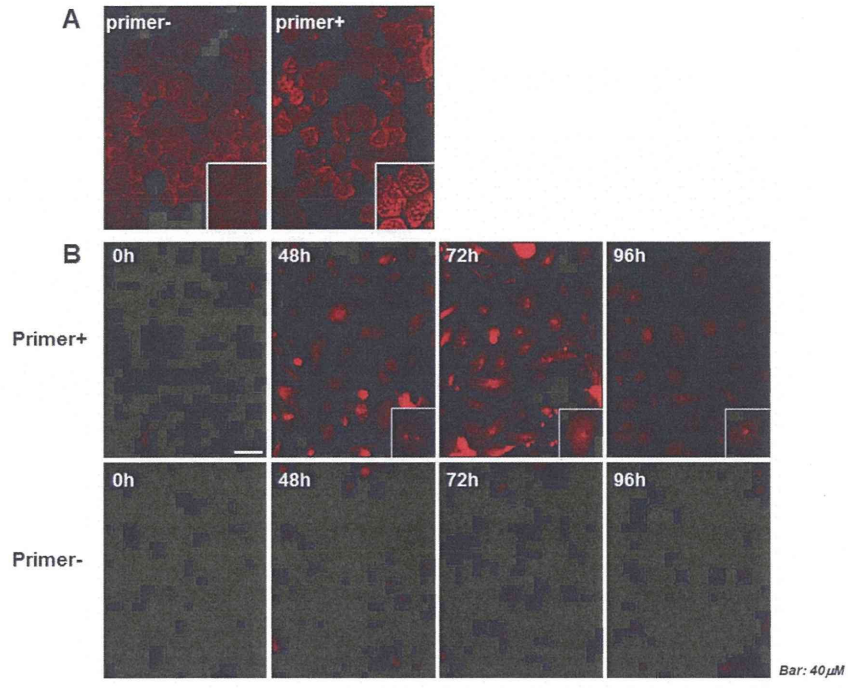

68x56mm (600 x 600 DPI)

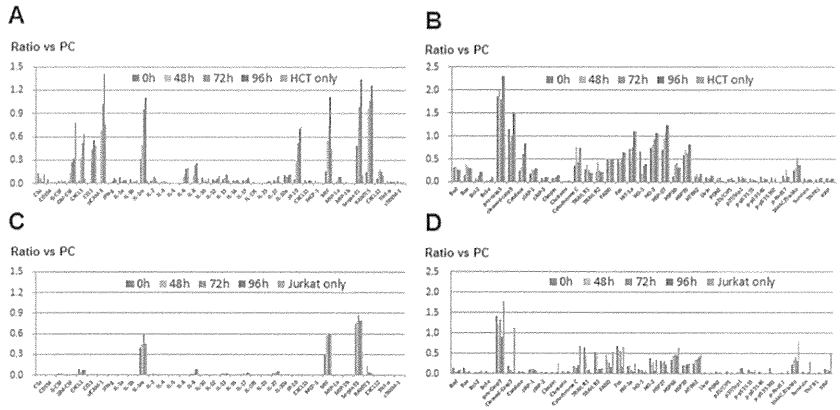

53x26mm (600 x 600 DPI)

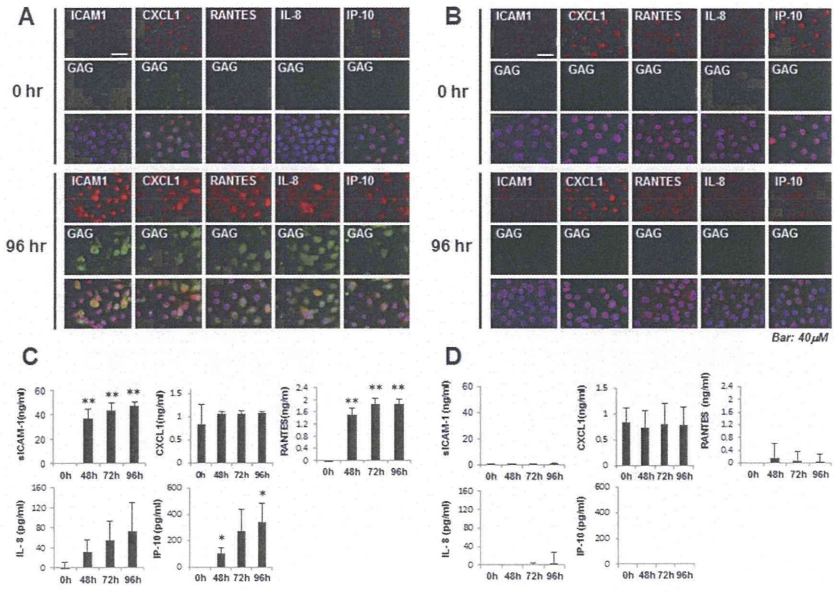

67x47mm (600 x 600 DPI)

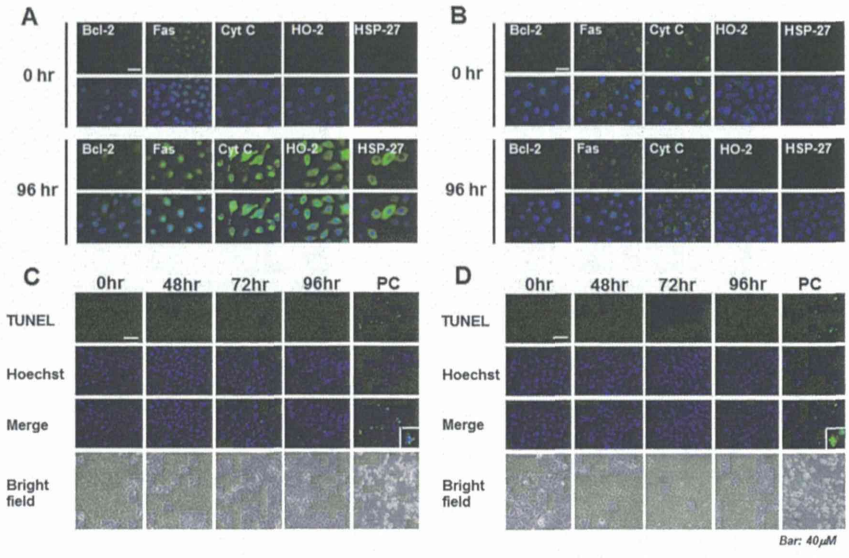

59x39mm (600 x 600 DPI)

TECHNIQUE

Pre-surround division technique: Precise cracks surrounding the posterior opacity prior to phacoemulsification in posterior polar cataract surgery

Koju Kamoi, MD, PhD, Manabu Mochizuki, MD, PhD

Three methods are currently used for posterior polar cataract surgery: intracapsular cataract extraction, posterior approach, and anterior approach. A high level of skill is required to divide the lens in the anterior approach, and few studies have investigated safer or simpler division methods. We focused on the division method in posterior polar cataract and developed a pre-surround division technique that divides the nucleus and avoids the posterior opacity. This technique creates precise cracks that surround the posterior opacity prior to phacoemulsification and does not cause intraoperative complications, resulting in successful intraocular lens implantation in all eyes. This pre-surround division method is a safe and easy technique that can be used in patients with posterior polar cataract.

Financial Disclosure: Neither author has a financial or proprietary interest in any material or method mentioned.

J Cataract Refract Surg 2014; 40:1764–1767 © 2014 ASCRS and ESCRS

Posterior polar cataract is associated with congenital defects in the posterior capsule. It has been reported in approximately 20% of cataract cases.[1] The major concern during cataract surgery is the presence of preexisting posterior capsule dehiscence at the center; therefore, ruptures of the posterior capsule frequently occur during surgery.[2,3] It is thus difficult for ophthalmologists to perform surgery safely in patients with posterior polar cataracts.

Three types of posterior polar cataract strategies are currently used: intracapsular cataract extraction, posterior approach, and anterior approach.[4] Many surgeons choose the anterior approach, as most posterior polar cataract cases have a soft nucleus (nuclear sclerosis <grade 2) and can be aspirated without dividing the nucleus. The inside-out delineation technique[5] has been used, particularly after a central trench is sculpted with the slow-motion technique.[6] This procedure demarcates the nucleus from the epinucleus and creates an epinucleus shell that helps in removal of the nucleus.

To perform phacoemulsification in elderly patients (nuclear sclerosis ≥grade 2), it is necessary to divide the nucleus so the lens can be removed.[4] Division procedures include conventional nucleus-dividing techniques such as divide and conquer,[7] phaco chop,[8] and step-by-step chop.[9] However, surgeons must be highly experienced as significant skill is required to prevent downward pressure on the posterior opacity.[10] In addition, inexperienced surgeons find that stable anterior chamber maintenance is not easy to achieve during the phacoemulsification phase. Although safe division is the key to a successful surgery, few reports in the literature provide details on a safe method of dividing the nucleus.

An accurate and easy method for creating cracks during the division prior to the phacoemulsification phase should improve the surgery and prevent these problems. We have developed a pre-surround division technique that uses the Akahoshi prechopper (ASICO

Submitted: March 1, 2014.
Final revision submitted: April 25, 2014.
Accepted: April 28, 2014.

From the Department of Ophthalmology and Visual Science, Graduate School of Medical and Dental Sciences, Tokyo Medical and Dental University, Tokyo, Japan.

Corresponding author: Koju Kamoi, MD, PhD, Department of Ophthalmology and Visual Science, Graduate School of Medical and Dental Sciences Tokyo Medical and Dental University, 1-5-45 Yushima, Bunkyo-ku, Tokyo 113-8519, Japan. E-mail: koju.oph@tmd.ac.jp.

http://dx.doi.org/10.1016/j.jcrs.2014.09.002
0886-3350

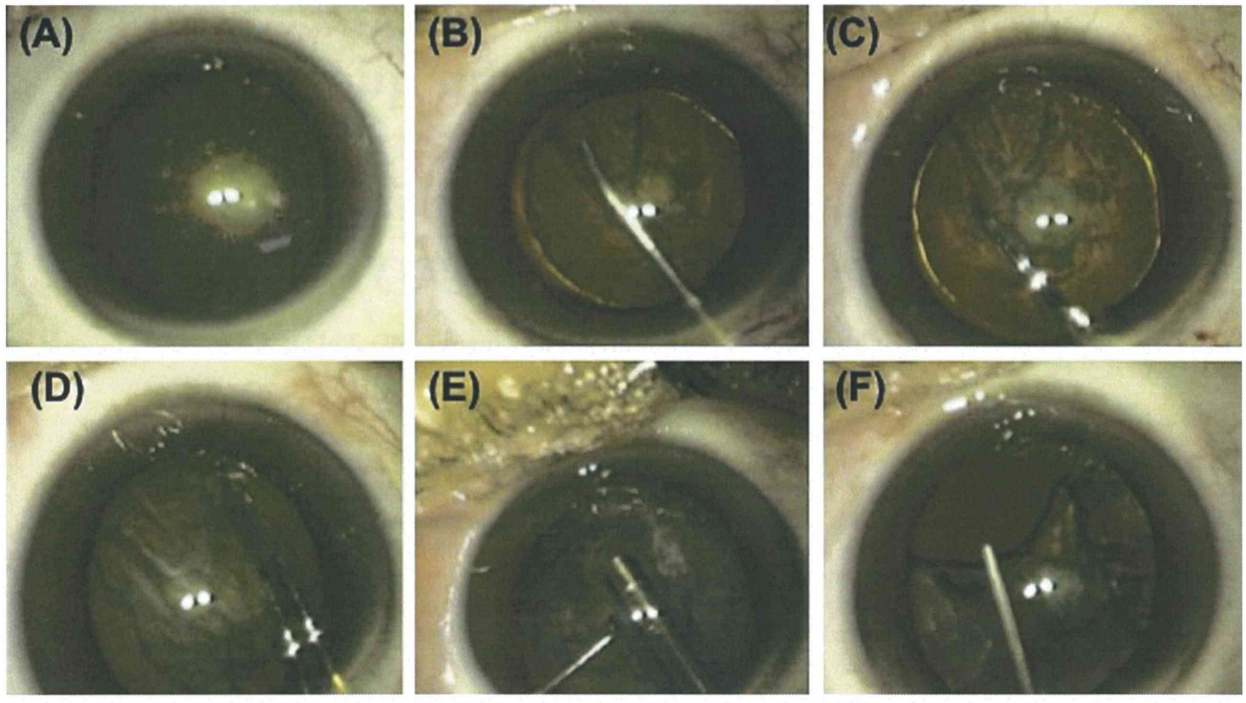

Figure 1. *A*: A round dense polar opacity is clearly seen. The opacity is located in the center of the posterior capsule. *B*: Hydrodelineation is performed as close to the center of the lens as possible. This leads to the creation of a golden ring. *C*: The first division by the Akahoshi prechopper is performed on the left side of the lens. The polar opacity is avoided during this division. *D*: The second pre-surround division is performed on the right side of the lens. Cracks that surround the polar opacity are created, ie, a pre-surround division. *E*: Phacoemulsification is performed with a hook. The center piece of the lens is shaved. During this procedure, the remaining side pieces help to keep the lens capsule stable. *F*: The OVD is slowly injected between the cortex and the posterior capsule.

LLC)[11] to divide the nucleus into 3 pieces. With this device, cracks that surround the centrally located posterior opacity are created prior to the phacoemulsification. This technique not only improves the safety of dividing the nucleus in posterior polar cataract patients, but can also be performed without the high level of skill required for other procedures.

SURGICAL TECHNIQUE

Phacoemulsification of the posterior polar cataract (Figure 1, *A*) is performed through a tunneled scleral incision with an ophthalmic viscosurgical device (OVD) placed in the anterior chamber using the soft-shell technique.[12] In this procedure, a dispersive OVD (Viscoat) is injected into the anterior chamber followed by a cohesive OVD (Opegan Hi). Over-insertion of the OVDs should be avoided because it can result in a breakdown of the posterior capsule.[10] Next, the anterior capsule is opened using the continuous curvilinear capsulorhexis (CCC) method.[13] To support a sulcus-fixated intraocular lens (IOL) or to enable optic capture through the anterior CCC in cases with posterior capsule rupture, a moderate-sized capsulorhexis is the preferred method. Subsequently, only hydrodelineation is performed and a golden ring is created as close to the center of the lens as possible (Figure 1, *B*). The cohesive OVD is inserted into the anterior chamber to maintain the space and facilitate easy division of the nucleus.

Prior to starting the phacoemulsification, an Akahoshi prechopper is used to chop and separate the lens nucleus into 3 pieces. To prevent the creation of cracks when using the pre-surround division technique, the polar opacity is avoided (Figure 1, *C* and *D*). The use of a moderate-sized capsulorhexis is also important to preserve the capsule's integrity. The first step of the phacoemulsification process is focused on the central piece of the divided lens. The side pieces of the divided lens help keep the capsule stable when the central piece is shaved. The side pieces of the lens are then shaved (Figure 1, *E*), which minimizes the movement of the posterior capsule during phacoemulsification. A hook is used throughout the phacoemulsification to prevent accidental separation of the polar opacity from the posterior capsule. After the entire nucleus of the lens is shaved, the dispersive OVD is slowly injected between the cortex and the posterior capsule. The OVD is then used to peel the cortex and the polar opacity from the posterior capsule (Figure 1, *F*). Finally, irrigation/aspiration (I/A) is performed while using the hook to remove the cortex and the polar opacity.

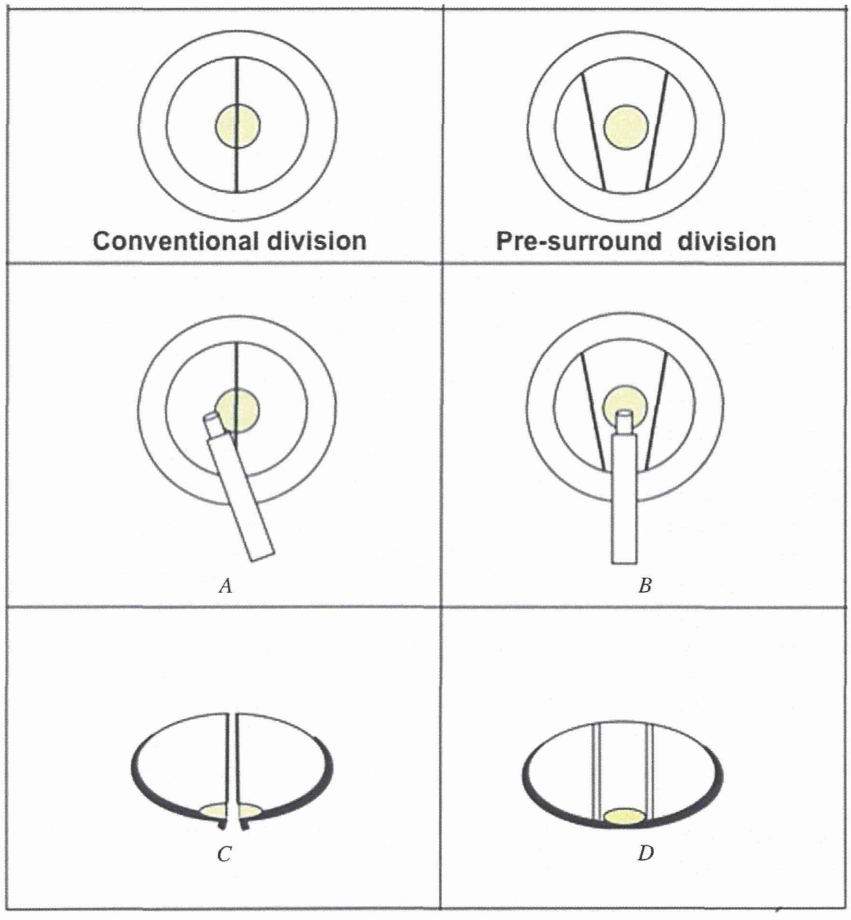

Figure 2. *A*: Conventional phacoemulsification techniques divide the lens into 2 pieces at the center. *B*: The pre-surround division technique divides the lens into 3 pieces without any rotation. *C*: The polar opacity strongly adheres to the posterior capsule. Thus, dividing the center of the lens often results in posterior capsule rupture when hydrodelineation is unsuccessful. *D*: The pre-surround division technique results in a safe division whether the hydrodelineation is successful or not.

Results

The pre-surround division technique was performed in 6 consecutive eyes of posterior polar cataract patients. The estimated nuclear sclerosis in these patients ranged from grade 2 to grade 3. No intraoperative complications were observed, and the IOLs were successfully implanted in all eyes. Although a congenital defect was found in 1 eye after the lens removal, no vitreous loss occurred. No postoperative complications such as dislocation of the IOLs were observed during the follow-up of at least 1 year.

DISCUSSION

One of the most important factors in posterior polar cataract surgery is removing the lens without moving the posterior capsule, which ensures that the polar opacity will be isolated until the end of the procedure. Most patients have a soft nucleus; therefore, cataract surgery can be performed using I/A rather than phacoemulsification. However, in elderly patients, phacoemulsification is usually required to remove the lens. The strategic methods required when removing the lens include hydrodelineation, rotation, and, particularly, division.

Dividing a nucleus over the posterior opacity with the conventional phaco procedure may reduce the safety of the surgery.[7–9] If a surgeon does not perform hydrodelineation to divide the nucleus of the posterior polar cataract correctly, both the nucleus and the polar opacity can be simultaneously divided, which leads to posterior capsule rupture (Figure 2, *C*).

Previously reported methods have shown that it is possible to divide the nucleus into more than 2 pieces, thereby avoiding the polar opacity during the phacoemulsification procedure.[3,14] However, these methods require a high level of skill to prevent the unintentional downward pressure on the posterior capsule that often occurs, and therefore they can be difficult to perform. To overcome the problems reported for these techniques and make the surgery easier to perform, we developed a pre-surround division technique that divides the nucleus into 3 pieces without rotating the

lens or creating cracks over the posterior opacity prior to starting the phacoemulsification process. Because the pieces of the nucleus generated by the pre-surround division technique are smaller than those created by the conventional technique and there is no rotation of the lens, it is markedly easier to control the overall process and shave the nucleus (Figure 2, *A* and *B*). Moreover, with this pre-surround division technique, the 2 pre-divisions prior to phacoemulsification can be easily performed with precision, avoiding the polar opacity (Figure 2, *D*). As a result, there is no danger of rupturing the posterior capsule with this technique, even if the hydrodelineation procedure is not performed perfectly. Although there are concerns that the lateral separating movement could threaten the capsule's integrity, the slow and lateral movement occurs away from the center, which helps to maintain the integrity. Although a prechopper can be used for a mild or moderately dense nucleus in most cases, it cannot be used for a hard dense nucleus. In addition to being safer and simpler to undertake, this new pre-surround division technique can be successfully used in cases in which standard phacoemulsification may not be applicable or may be too difficult to perform.

WHAT WAS KNOWN

- The presence of preexisting posterior capsule dehiscence at the center of a posterior capsule cataract can result in rupture of the posterior capsule.
- There are few reports on the safe method of dividing the nucleus in posterior polar cataract.

WHAT THIS PAPER ADDS

- The pre-surround division technique divides the posterior polar cataract nucleus into 3 pieces without rotating the lens or creating cracks over the posterior opacity prior to phacoemulsification.

REFERENCES

1. Osher RH, Yu BC-Y, Koch DD. Posterior polar cataracts: a predisposition to intraoperative posterior capsular rupture. J Cataract Refract Surg 1990; 16:157–162
2. Hayashi K, Hayashi H, Nakao F, Hayashi F. Outcomes of surgery for posterior polar cataract. J Cataract Refract Surg 2003; 29:45–49
3. Vasavada A, Singh R. Phacoemulsification in eyes with posterior polar cataract. J Cataract Refract Surg 1999; 25:238–245
4. Vasavada AR, Raj SM, Vasavada V, Shrivastav S. Surgical approaches to posterior polar cataract: a review. Eye 2012; 26:761–770. Available at: http://www.ncbi.nlm.nih.gov/pmc/articles/PMC3376282/pdf/eye201233a.pdf. Accessed May 3, 2014
5. Vasavada AR, Raj SM. Inside-out delineation. J Cataract Refract Surg 2004; 30:1167–1169
6. Osher RH. Slow motion phacoemulsification approach [letter]. J Cataract Refract Surg 1993; 19:667
7. Gimbel HV. Divide and conquer nucleofractis phacoemulsification: development and variations. J Cataract Refract Surg 1991; 17:281–291
8. Fine IH. The chip and flip phacoemulsification technique. J Cataract Refract Surg 1991; 17:366–371
9. Vasavada AR, Singh R. Step-by-step chop in situ and separation of very dense cataracts. J Cataract Refract Surg 1998; 24: 156–159
10. Fine IH, Packer M, Hoffman RS. Management of posterior polar cataract. J Cataract Refract Surg 2003; 29:16–19
11. Akahoshi T. Phaco prechop: manual nucleofracture prior to phacoemulsification. Operative Tech Cataract Refract Surg 1998; 1:69–91
12. Arshinoff SA. Dispersive-cohesive viscoelastic soft shell technique. J Cataract Refract Surg 1999; 25:167–173
13. Gimbel HV, Neuhann T. Continuous curvilinear capsulorhexis. J Cataract Refract Surg 1991; 17:110–111
14. Chee S-P. Management of the hard posterior polar cataract. J Cataract Refract Surg 2007; 33:1509–1514

First author:
Koju Kamoi, MD, PhD

Department of Ophthalmology and Visual Science, Graduate School of Medical and Dental Sciences, Tokyo Medical and Dental University, Tokyo, Japan

HTLV-1 induces a Th1-like state in CD4$^+$CCR4$^+$ T cells

Natsumi Araya,[1] Tomoo Sato,[1] Hitoshi Ando,[1] Utano Tomaru,[2] Mari Yoshida,[3] Ariella Coler-Reilly,[1] Naoko Yagishita,[1] Junji Yamauchi,[1] Atsuhiko Hasegawa,[4] Mari Kannagi,[4] Yasuhiro Hasegawa,[5] Katsunori Takahashi,[1] Yasuo Kunitomo,[1] Yuetsu Tanaka,[6] Toshihiro Nakajima,[7,8] Kusuki Nishioka,[7] Atae Utsunomiya,[9] Steven Jacobson,[10] and Yoshihisa Yamano[1]

[1]Department of Rare Diseases Research, Institute of Medical Science, St. Marianna University School of Medicine, Kanagawa, Japan. [2]Department of Pathology, Hokkaido University Graduate School of Medicine, Hokkaido, Japan. [3]Institute for Medical Science of Aging, Aichi Medical University, Aichi, Japan. [4]Department of Immunotherapeutics, Tokyo Medical and Dental University, Graduate School, Tokyo, Japan. [5]Department of Neurology, St. Marianna University School of Medicine, Kanagawa, Japan. [6]Department of Immunology, Graduate School of Medicine, University of the Ryukyus, Okinawa, Japan. [7]Institute of Medical Science and [8]Center for Clinical Research, Tokyo Medical University, Tokyo, Japan. [9]Department of Hematology, Imamura Bun-in Hospital, Kagoshima, Japan. [10]Viral Immunology Section, Neuroimmunology Branch, National Institutes of Health, Bethesda, Maryland, USA.

Human T-lymphotropic virus type 1 (HTLV-1) is linked to multiple diseases, including the neuroinflammatory disease HTLV-1–associated myelopathy/tropical spastic paraparesis (HAM/TSP) and adult T cell leukemia/lymphoma. Evidence suggests that HTLV-1, via the viral protein Tax, exploits CD4$^+$ T cell plasticity and induces transcriptional changes in infected T cells that cause suppressive CD4$^+$CD25$^+$CCR4$^+$ Tregs to lose expression of the transcription factor FOXP3 and produce IFN-γ, thus promoting inflammation. We hypothesized that transformation of HTLV-1–infected CCR4$^+$ T cells into Th1-like cells plays a key role in the pathogenesis of HAM/TSP. Here, using patient cells and cell lines, we demonstrated that Tax, in cooperation with specificity protein 1 (Sp1), boosts expression of the Th1 master regulator T box transcription factor (T-bet) and consequently promotes production of IFN-γ. Evaluation of CSF and spinal cord lesions of HAM/TSP patients revealed the presence of abundant CD4$^+$CCR4$^+$ T cells that coexpressed the Th1 marker CXCR3 and produced T-bet and IFN-γ. Finally, treatment of isolated PBMCs and CNS cells from HAM/TSP patients with an antibody that targets CCR4$^+$ T cells and induces cytotoxicity in these cells reduced both viral load and IFN-γ production, which suggests that targeting CCR4$^+$ T cells may be a viable treatment option for HAM/TSP.

Introduction

The flexibility of the CD4$^+$ T cell differentiation program that underlies the success of the adaptive immune response has recently been implicated in the pathogeneses of numerous inflammatory diseases (1–3). The majority of CD4$^+$ T lymphocytes belong to a class of cells known as Th cells, so called because they provide help on the metaphorical immune battlefield by stimulating the other soldiers — namely, B cells and cytotoxic T lymphocytes — via secretion of various cytokines. Interestingly, there is also a minority group of CD4$^+$ T cells with quite the opposite function: Tregs actively block immune responses by suppressing the activities of CD4$^+$ Th cells as well as many other leukocytes (4). Tregs are credited with maintaining immune tolerance and preventing inflammatory diseases that could otherwise occur as a result of uninhibited immune reactions (5). Thus, the up- or downregulation of certain CD4$^+$ T cell lineages could disrupt the carefully balanced immune system, threatening bodily homeostasis.

The plasticity of CD4$^+$ T cells, particularly Tregs, makes CD4$^+$ T cell lineages less clean-cut than they may originally appear. CD4$^+$ T cells are subdivided according to various lineage-specific chemokine receptors and transcription factors they express, as well as the cytokines they produce (6). Th1 cells, for example, can be identified by expression of CXC motif receptor 3 (CXCR3) and T box transcription factor (T-bet; encoded by *TBX21*) and are known to secrete the proinflammatory cytokine IFN-γ (6). While both have been known to express CC chemokine receptor 4 (CCR4) and CD25, Th2 cells and Tregs can usually be distinguished from each other by their expression of GATA-binding protein 3 (GATA3) and forkhead box p3 (FOXP3), respectively (6, 7). CCR4 is coexpressed in the majority of CD4$^+$FOXP3$^+$ cells and in virtually all CD4$^+$CD25$^+$FOXP3$^+$ cells, making it a useful — albeit not fully specific — marker for Tregs (8, 9). FOXP3 is a particularly noteworthy marker because its expression is said to be required for Treg identity and function (10). In fact, *Foxp3* point mutations are reported to cause fatal multiorgan autoimmune diseases (11). Even partial loss of FOXP3 expression can disrupt the suppressive nature of Tregs, representing one of several pathways by which even fully differentiated Tregs can reprogram into inflammatory cells (12). There have been several reports of Tregs reprogramming in response to proinflammatory cytokines such as IL-1, IL-6, IL-12, and IFN-γ (12, 13); it is thought that this reprogramming may have evolved as an adaptive mechanism for dampening immune suppression when protective inflammation is necessary (12). However, this same plasticity can lead to pathologically chronic inflammation, and several autoimmune diseases have been associated with reduced FOXP3 expression and/or Treg function, including multiple sclerosis, myasthenia gravis, and type 1 diabetes (14, 15).

Of the roughly 10–20 million people worldwide infected with human T-lymphotropic virus type 1 (HTLV-1), up to 2%–3% are affected by the neurodegenerative chronic inflammatory dis-

Conflict of interest: The authors have declared that no conflict of interest exists.
Submitted: January 17, 2014; **Accepted:** May 8, 2014.
Reference information: *J Clin Invest.* 2014;124(8):3431–3442. doi:10.1172/JCI75250.

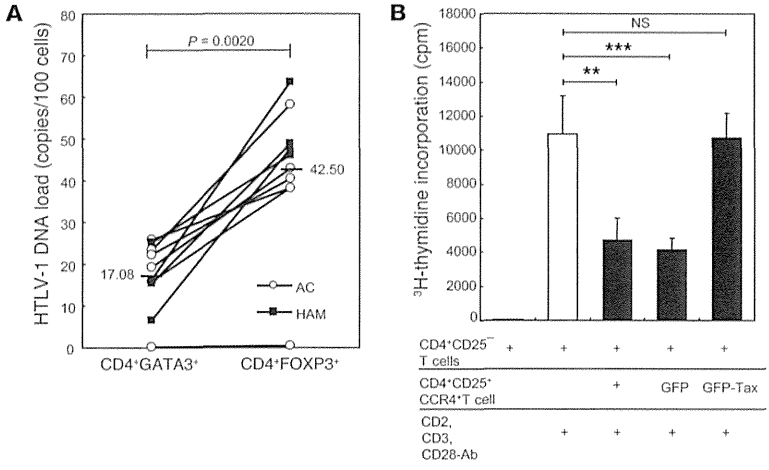

Figure 1. HTLV-1 mainly infects Tregs and inhibits their regulatory function. (**A**) Higher HTLV-1 proviral DNA load in CD4⁺FOXP3⁺ cells (Tregs) compared with CD4⁺GATA3⁺ cells ($P = 0.0020$, Wilcoxon test) from asymptomatic carriers (AC; $n = 6$) and HAM/TSP patients ($n = 4$). PBMCs were FACS sorted, and proviral load was measured using quantitative PCR. Horizontal bars represent the mean value for each set. (**B**) Loss of regulatory function in Tax-expressing CD4⁺CD25⁺CCR4⁺ cells (Tregs). CD4⁺CD25⁻ T cells from an HD were stimulated with CD2, CD3, and CD28 antibodies and cultured alone or in the presence of equal numbers of CD4⁺CD25⁺CCR4⁺ T cells, GFP lentivirus-infected HD CD4⁺CD25⁺CCR4⁺ T cells, or GFP-Tax lentivirus-infected HD CD4⁺CD25⁺CCR4⁺ T cells. As a control, CD4⁺CD25⁻ T cells alone were cultured without any stimulus. Proliferation of T cells was determined using ^{3}H-thymidine incorporation by adding ^{3}H-thymidine for 16 hours after 4 days of culture. All tests were performed in triplicate. Data are mean ± SD. $^{**}P < 0.01$, $^{***}P < 0.001$, ANOVA followed by Tukey test for multiple comparisons.

ease HTLV-1–associated myelopathy/tropical spastic paraparesis (HAM/TSP). The main other condition associated with the retrovirus is adult T cell leukemia/lymphoma (ATLL), a rare and aggressive cancer of the T cells. HAM/TSP represents a useful starting point from which to investigate the origins of chronic inflammation, because the primary cause of the disease — viral infection — is so unusually well defined. HAM/TSP patients share many immunological characteristics with FOXP3 mutant mice, including multiorgan lymphocytic infiltrates, overproduction of inflammatory cytokines, and spontaneous lymphoproliferation of cultured CD4⁺ T cells (16–18). We and others have proposed that HTLV-1 preferentially infects CD4⁺CD25⁺CCR4⁺ T cells, a group that includes Tregs (7, 19). Samples of CD4⁺CD25⁺CCR4⁺ T cells isolated from HAM/TSP patients exhibited low FOXP3 expression as well as reduced production of suppressive cytokines and low overall suppressive ability — in fact, these CD4⁺CD25⁺CCR4⁺FOXP3⁻ T cells were shown to produce IFN-γ and express Ki67, a marker of cell proliferation (19). The frequency of these IFN-γ–producing CD4⁺CD25⁺CCR4⁺ T cells in HAM/TSP patients was correlated with disease severity (19). Finally, evidence suggests that the HTLV-1 protein product Tax may play a role in this alleged transformation of Tregs into proinflammatory cells in HAM/TSP patients: transfecting Tax into CD4⁺CD25⁺ cells from healthy donors (HDs) reduced FOXP3 mRNA expression, and Tax expression in CD4⁺CD25⁺CCR4⁺ cells was higher in HAM/TSP versus ATLL patients despite similar proviral loads (19, 20). Therefore, we hypothesized that HTLV-1 causes chronic inflammation by infecting CD4⁺CD25⁺CCR4⁺ T cells and inducing their transformation into Th1-like, IFN-γ–producing proinflammatory cells via intracellular Tax expression and subsequent transcriptional alterations including but not limited to loss of endogenous FOXP3 expression.

In this study, we first sought to discover the detailed mechanism by which Tax influences the function of CD4⁺CD25⁺CCR4⁺ T cells. We used DNA microarray analysis of CD4⁺CD25⁺CCR4⁺ T cells from HAM/TSP patients to identify *TBX21*, known as a master transcription factor for Th1 differentiation, as a key intermediary between Tax expression and IFN-γ production. We demonstrated that Tax, in concert with specificity protein 1 (Sp1), amplified *TBX21* transcription and subsequently IFN-γ production. Next, we established the presence of Th1-like CD4⁺CCR4⁺ T cells in the CSF and spinal cord lesions of HAM/TSP patients. The majority of these CD4⁺CCR4⁺ T cells coexpressed CXCR3 as well as T-bet and IFN-γ. Finally, we investigated the therapeutic potential of an anti-CCR4 monoclonal antibody with antibody-dependent cellular cytotoxicity (ADCC) (21). Applying this antibody in vitro diminished the proliferative capacity of cultured PBMCs and reduced both proviral DNA load and IFN-γ production in cultured CSF cells as well as PBMCs. In conclusion, we were able to elucidate a more detailed mechanism for the pathogenesis of HAM/TSP and use our findings to suggest a possible therapeutic strategy.

Results

HTLV-1 preferentially infects Tregs and alters their behavior via Tax. Experiments were conducted to determine which among CD4⁺CD25⁺CCR4⁺ T cells were infected by HTLV-1, and how the infection influenced their functionality. Analysis of fluorescence-activated cell sorting (FACS)-sorted PBMCs obtained from asymptomatic carriers ($n = 6$) as well as HAM/TSP patients ($n = 4$) revealed that Tregs (CD4⁺FOXP3⁺) carried much higher proviral loads than Th2 cells (CD4⁺GATA3⁺) ($P = 0.0020$; Figure 1A). As it is well established that each infected cell contains only 1 copy of the HTLV-1 provirus (22, 23), these results indicate that a larger proportion of FOXP3⁺ than GATA3⁺ CD4⁺ T cells are infected. As expected, proliferation of CD4⁺CD25⁻ cells after stimulation, as measured by ^{3}H-thymidine incorporation, was suppressed upon coculture with CD4⁺CD25⁺CCR4⁺ cells, including Tregs ($n = 3$, $P < 0.01$; Figure 1B). However, after being transduced with lentiviral vector expressing GFP-Tax, the CD4⁺CD25⁺CCR4⁺ cells no longer suppressed cell proliferation; conversely, cells transduced with the control vector expressing only GFP retained full suppressive function ($P < 0.001$; Figure 1B).

The HTLV-1 protein product Tax induces IFN-γ production via T-bet. Experiments were conducted to determine if and how Tax affects IFN-γ production in infected T cells. First, the existence of a functional link between *Tax* and *IFNG* was established by using the

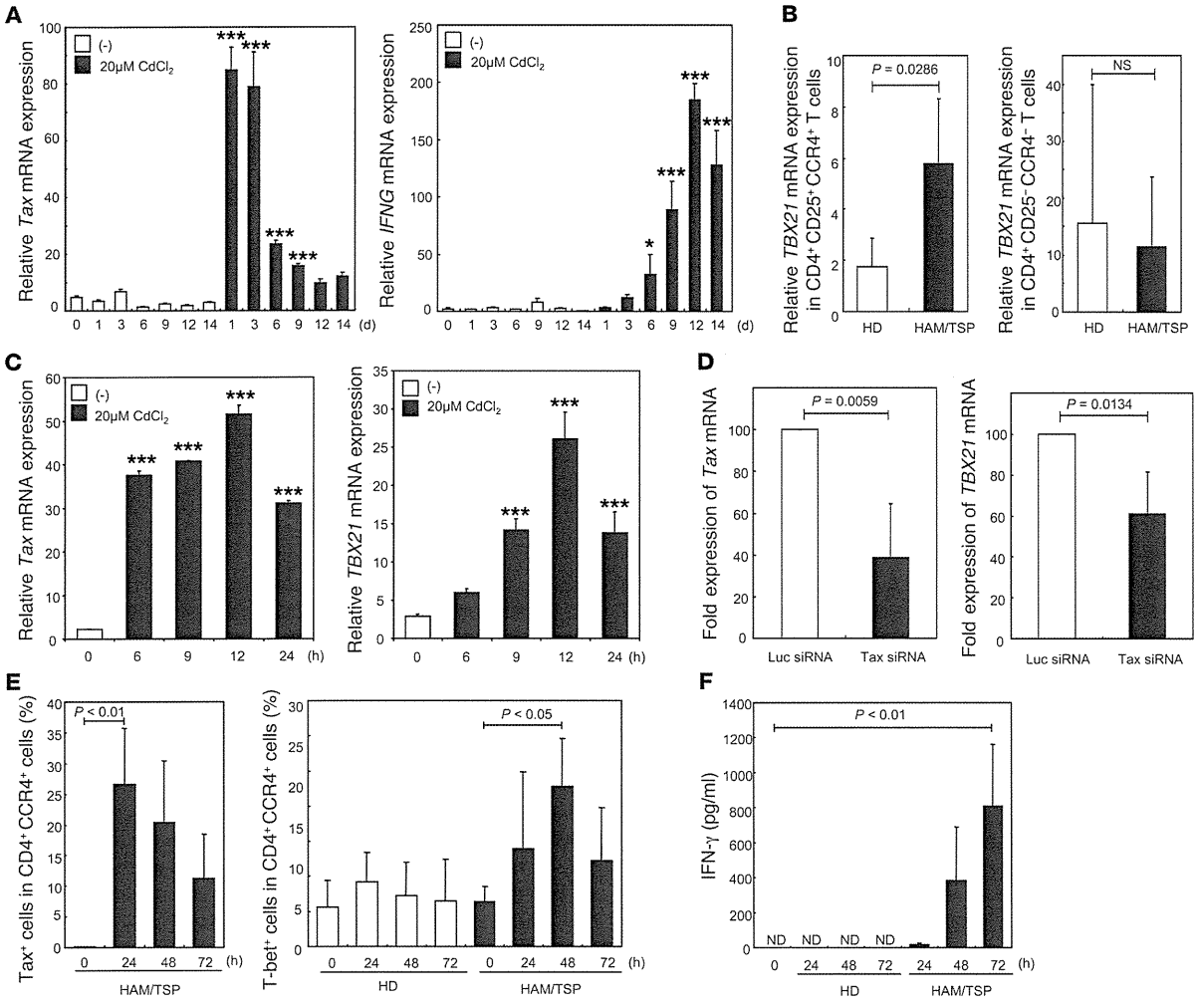

Figure 2. Tax induces IFN-γ production via T-bet. (**A**) Tax-dependent *IFNG* mRNA expression in JPX-9 cells. Experiments were performed in triplicate. (**B**) Elevated *TBX21* mRNA expression in $CD4^+CD25^+CCR4^+$ T cells from HAM/TSP patients relative to HDs ($n = 4$ per group). (**C**) Tax-dependent *TBX21* mRNA expression in JPX-9 cells. Experiments were performed in triplicate. (**D**) Reduced *TBX21* mRNA expression after silencing Tax in $CD4^+CD25^+CCR4^+$ T cells from HAM/TSP patients. PBMCs from HAM/TSP patients ($n = 5$) were FACS sorted, transfected with either Luc or Tax siRNA, and incubated for 24 hours. (**E** and **F**) Tax expression correlated with T-bet expression and IFN-γ production in $CD4^+CCR4^+$ T cells from HAM/TSP patients. $CD4^+CCR4^+$ T cells isolated from HDs and HAM/TSP patients ($n = 4$ per group) were cultured before being stained for Tax and T-bet protein and analyzed using FACS. IFN-γ production in the culture medium was measured using a CBA assay. ND, not detectable. All data are mean ± SD. *P* values were calculated using (**A** and **C**) 1-way ANOVA followed by Dunnett test for multiple comparisons, (**B**) Mann-Whitney *U* test, (**D**) paired *t* test, or (**E** and **F**) Friedman test followed by Dunn test for multiple comparisons. $^*P < 0.05$, $^{***}P < 0.001$ vs. time point 0.

JPX-9 cell line possessing a stably integrated $CdCl_2$-inducible *Tax* construct and measuring *IFNG* mRNA expression. Inducing *Tax* expression with $CdCl_2$ periodically over 2 weeks yielded a steady rise in *IFNG* expression (Figure 2A). Although there was clearly a correlation between Tax and IFN-γ expression, the *IFNG* expression level was not proportional to that of *Tax*, and the steepest rise in the former was delayed several days after the steepest rise in the latter. Thus, we suspected that expression of 1 or more additional genes may represent an important middle step on the pathway linking Tax and IFN-γ production. DNA microarray results revealed that expression of *TBX21*, which is known to be associated with IFN-γ production, was elevated in $CD4^+CD25^+CCR4^+$ cells from the HAM/TSP patient, but not the ATLL patient, compared with the HD (Supplemental Figure 1; supplemental material available online with this article; doi:10.1172/JCI75250DS1). *TBX21* mRNA expression, measured via real-time RT-PCR, was elevated in $CD4^+CD25^+CCR4^+$ cells, but not $CD4^+CD25^-CCR4^-$ cells, from HAM/TSP patients compared with HDs (Figure 2B). A direct correlation between *Tax* and *TBX21* mRNA expression was then established using the JPX-9 cell line, as described above (Figure 2C). Silencing the *Tax* gene with siRNA in $CD4^+CD25^+CCR4^+$ cells from HAM/TSP patients reduced *TBX21* as well as *Tax* expression (Figure 2D). Similarly,

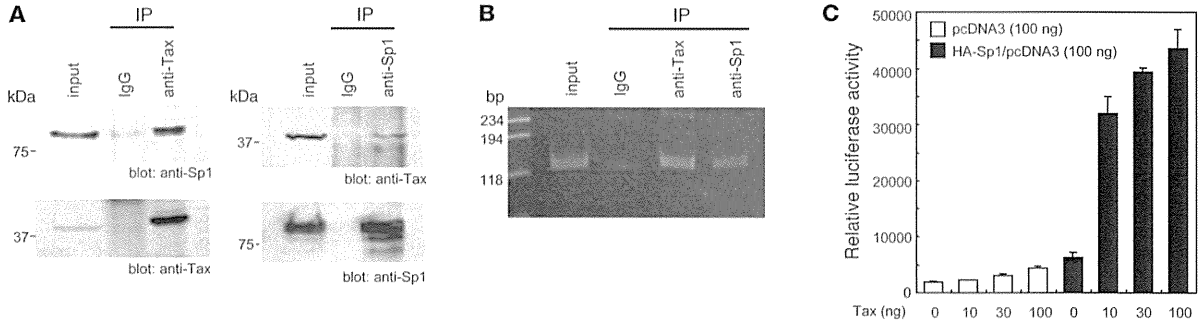

Figure 3. Tax and Sp1 cooperatively enhance *TBX21* promoter activity. (**A**) Co-IP of endogenous Tax and Sp1. Nuclear extracts from MT-2 cells were immunoprecipitated with anti-Tax or anti–Sp1 antibodies or with normal IgG as a control, then immunoblotted with anti-Tax or anti-Sp1 antibodies as indicated. (**B**) Tax bound to the *TBX21* promoter in vivo. ChIP assay using anti-Tax antibody followed by primers encompassing the *TBX21* promoter region (–179 to –59) was performed on genomic DNA isolated from MT-2 cells. DNA (input) and IP with anti-Sp1 served as positive controls, and normal IgG served as a negative control. (**C**) Coactivation of *TBX21* promoter by Sp1 and Tax. HEK293 cells were transfected with 100 ng of *TBX21*-Luc reporter plasmid or Sp1 expression plasmid, as well as 0–100 ng of Tax expression plasmid as indicated. Values were normalized to β-galactosidase activity as an internal control. Data are mean ± SD.

elevation of *Tax* expression via transduction of a GFP-Tax construct into $CD4^+CD25^+CCR4^+$ cells from a HD increased expression of *TBX21* as well as *Tax* (Supplemental Figure 2). Thus, a functional relationship between *Tax* and *TBX21* was confirmed. Finally, among $CD4^+CCR4^+$ cells from HAM/TSP patients, the appearance of Tax^+ cells was associated with a rise in the percentage of $T\text{-}bet^+$ cells, which was associated with a delayed but roughly proportional rise in the amount of IFN-γ protein (Figure 2, E and F). The production of Tax versus T-bet in these $CD4^+CCR4^+$ cells from HAM/TSP patients was compared at 0 versus 48 hours of culturing. At 0 hours, the overwhelming majority of the $CD4^+CCR4^+$ cells were both Tax^- and $T\text{-}bet^-$; by 48 hours, a substantial presence of $Tax^+T\text{-}bet^+$ cells had emerged, and there were very few $T\text{-}bet^+$ cells that were not also Tax^+ (Supplemental Figure 3).

Tax in concert with Sp1 induces TBX21 transcription. Experiments were conducted to investigate the mechanism by which Tax may be involved in *TBX21* transcription in HTLV-1–infected T cells. First, co-IP reactions were performed using nuclear extracts from the HTLV-1–infected MT-2 T cell line to confirm a suspected interaction between endogenous Tax and Sp1, which is known to both form a complex with Tax and to activate *TBX21* transcription (24, 25). Precipitation with anti-Tax or anti-Sp1 antibodies yielded bands corresponding to both Tax and Sp1, whereas precipitation with the nonspecific IgG antibody as the negative control yielded neither band (Figure 3A), thus demonstrating the existence of a Tax-Sp1 complex in HTLV-1–infected T cells. Second, a ChIP assay using primers encompassing the *TBX21* promoter region (–179 to –59) was performed on the MT-2 cells to confirm the suspected interaction between this Tax-Sp1 complex and the *TBX21* promoter. Precipitation with anti-Tax or anti-Sp1, but not IgG, yielded a PCR product corresponding to the *TBX21* promoter (Figure 3B), which suggests that a Tax-Sp1 complex does bind to the *TBX21* promoter site. Finally, a reporter assay was performed using cells transfected with *TBX21*-Luc, a luciferase reporter plasmid containing the *TBX21* promoter region, to confirm a functional relationship among Tax, Sp1, and *TBX21* transcription. Cotransfection with Sp1 resulted in elevated luciferase activity compared with transfection with the reporter alone, and addition of Tax heightened this effect in a concentration-dependent manner (Figure 3C). These findings suggested that Tax, in concert with Sp1, induces *TBX21* transcription.

HTLV-1–infected Th1-like $CCR4^+$ cells are in the CNS of HAM/TSP patients. We next sought to confirm that HTLV-1–infected $CCR4^+$ T cells infiltrate the spinal cords of HAM/TSP patients and exhibit Th1-like traits, such as T-bet and IFN-γ production. Fluorescent immunohistochemical staining of tissue sections from HAM/TSP patient spinal cord lesions revealed the presence of abundant $CCR4^+$ cells infiltrating around the small blood vessels and coexpressing T-bet and IFN-γ (Figure 4A and Supplemental Figure 4). Further investigation revealed that these $CCR4^+$ cells also expressed CXCR3, the marker for Th1 cells (6). It should be noted that both IFN-γ and CXCR3 expression are reported to be induced by T-bet expression (6). Immunofluorescent staining was also used to demonstrate the existence of HTLV-1–infected $CCR4^+$ cells in the CSF of HAM/TSP patients (Figure 4B). $CCR4^+CXCR3^+$ cells were numerous among cells isolated from the CSF of HAM/TSP patients, representing 73.90% of $CD4^+$ cells isolated from a representative patient (Figure 4C) and 63.63% ± 6.73% of $CD4^+$ cells isolated from all patients ($n = 8$; Figure 4D). However, nearly all of these $CD4^+CCR4^+CXCR3^+$ cells were negative for Ki67, a marker of cell proliferation, in the CSF of the HAM/TSP patients (93.94% ± 2.07%, $n = 3$; Figure 4E). The majority of these $CD4^+CCR4^+CXCR3^+$ cells were also $CD25^+$ (70.16% ± 14.08%, $n = 3$, Supplemental Figure 5), confirming the existence of a substantial $CD4^+CD25^+CCR4^+CXCR3^+$ cell population in the CSF of HAM/TSP patients. Importantly, $CD4^+CCR4^+CXCR3^+$ cells did not make up the majority of PBMCs in HAM/TSP patients nor in HDs; in fact, such cells were very few (HAM/TSP, 3.65% ± 1.96%, $n = 8$; HD, 6.88% ± 3.09%, $n = 4$; Figure 4D). PBMCs were also isolated from ATLL patients for comparison, and $CD4^+CCR4^+CXCR3^-$ cells made up the overwhelming majority (83.03% ± 18.61%, $n = 5$; Supplemental Figure 6).

CCR4 shows potential as a molecular target for HAM/TSP immunotherapy. Analysis of HTLV-1 proviral DNA load in subpopulations of $CD4^+$ PBMCs from HAM/TSP patients confirmed that $CCR4^+$ cells were heavily infected, compared with less than

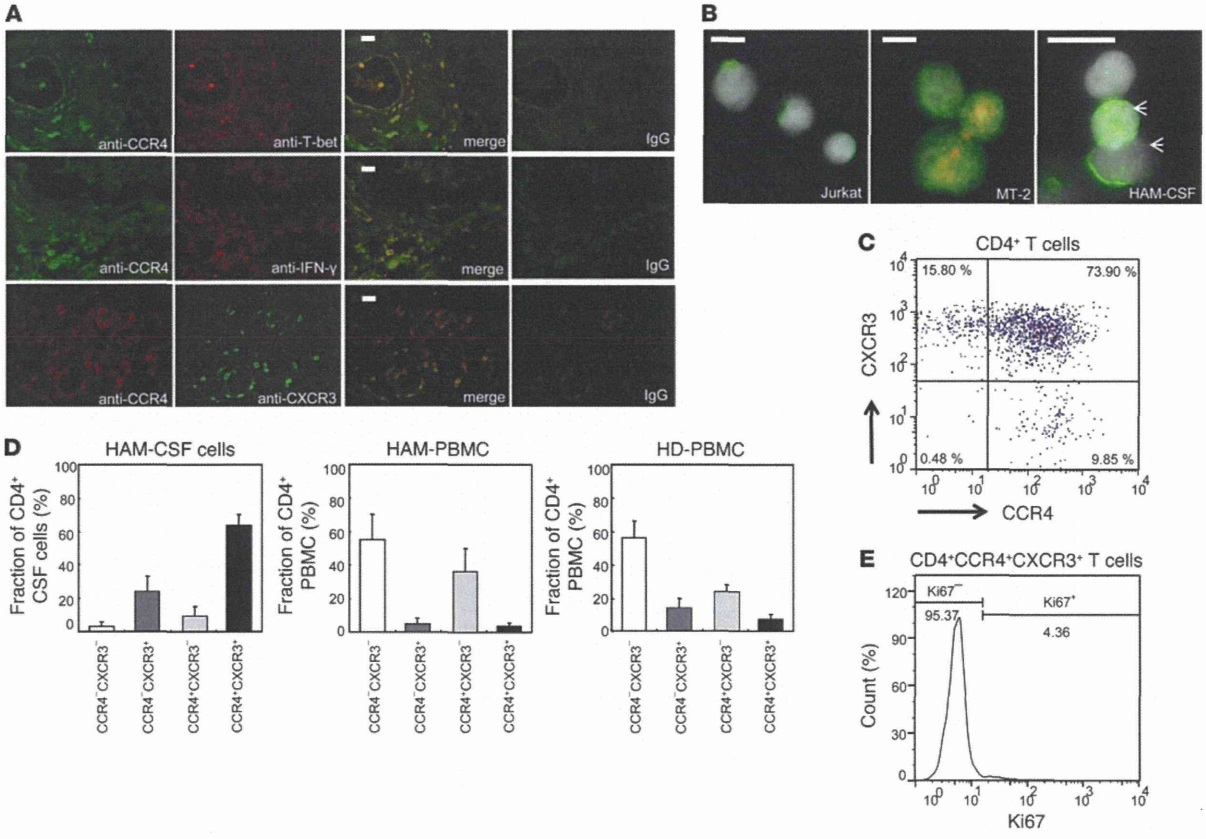

Figure 4. HTLV-1–infected Th1-like CCR4⁺ cells invade the CNS of HAM/TSP patients. (**A**) Detection of CCR4⁺ cells expressing T-bet, IFN-γ, and CXCR3 infiltrating the spinal cord of a HAM/TSP patient. Representative images show immunofluorescent codetection of CCR4 with T-bet, IFN-γ, and CXCR3, as well as the merged images, in thoracic spinal cord sections. Rabbit and goat IgG antibody served as a negative control. Scale bars: 20 μm. (**B**) Presence of HTLV-1–infected CCR4⁺ cells in HAM/TSP patient CSF. Representative images show immunofluorescence-FISH codetection of CCR4 (green) and HTLV-1 provirus (red) in Jurkat cells (uninfected control), MT-2 cells (infected control), and CSF cells from the patients. Arrows denote red provirus signal in the CSF sample. Scale bars: 20 μm. (**C**) CD4⁺ T cells in HAM/TSP patient CSF were mostly $CCR4^+CXCR3^+$. A dot plot of CCR4 and CXCR3 expression in CD4⁺ gated cells isolated from the CSF of a representative HAM/TSP patient is shown. (**D**) $CD4^+CCR4^+CXCR3^+$ cells were numerous in CSF, but not elevated in peripheral blood, of HAM/TSP patients. Graphs show the percentages of $CCR4^-CXCR3^-$, $CCR4^-CXCR3^+$, $CCR4^+CXCR3^-$ and $CCR4^+CXCR3^+$ T cells among CD4⁺ PBMCs and CSF cells from HAM/TSP patients ($n = 8$) and PBMCs from HDs ($n = 4$). Analysis was performed using FACS. Data are mean ± SD. (**E**) Proliferation was not observed in $CD4^+CCR4^+CXCR3^+$ cells from HAM/TSP patient CSF. The rate of Ki67 expression, a marker for cell proliferation, is shown for $CD4^+CCR4^+CXCR3^+$ gated cells from the CSF of a representative HAM/TSP patient.

1% of $CCR4^-$ cells ($n = 7$; Figure 5A). To predict the efficacy of a $CCR4^+$ cell–targeting cytotoxic antibody as a treatment for HAM/TSP, PBMCs were isolated from patients ($n = 9$) and analyzed after being cultured with and without the defucosylated chimeric anti-CCR4 monoclonal antibody KM2760 (21) or, for comparison, the steroid therapy prednisolone (PSL). Addition of 1 μg/ml KM2760 significantly reduced the percentage of $CCR4^+$ cells, as measured after 7 days ($P = 0.0039$; Figure 5B). As little as 0.1 μg/ml KM2760 was necessary to reduce the HTLV-1 DNA load ($P < 0.05$), whereas PSL had no significant impact (Figure 5C). Use of 1 μg/ml of either KM2760 or PSL was sufficient to suppress spontaneous proliferation of the PBMCs, as measured by ^{3}H-thymidine incorporation ($P < 0.05$ and $P < 0.01$, respectively; Figure 5D) as well as IFN-γ production ($P < 0.05$ and $P < 0.001$, respectively; Figure 5E). Similar results were observed in experiments using cells isolated from the CSF of HAM/TSP patients ($n = 8$): cultures to which 1 μg/ml of KM2760 had been added exhibited reduced HTLV-1 DNA load ($P = 0.0078$; Figure 5F) and IFN-γ production ($P = 0.0391$; Figure 5G). Certain samples shown in Figure 5G did not exhibit this reduction in IFN-γ production; those samples had particularly low cell counts (0.33–2.00 cells/μl), yielding less reliable data. Despite the presence of those lower-quality samples, statistical significance was still established for the sample group as a whole.

Discussion

Previously, we hypothesized that HTLV-1 gives rise to HAM/TSP by altering the behavior of infected cells via Tax expression to yield a new population of Th1-like proinflammatory cells (26). Evidence indicated that a significant portion of this population might be Tregs, as suggested by the $CD4^+CD25^+CCR4^+$ expres-

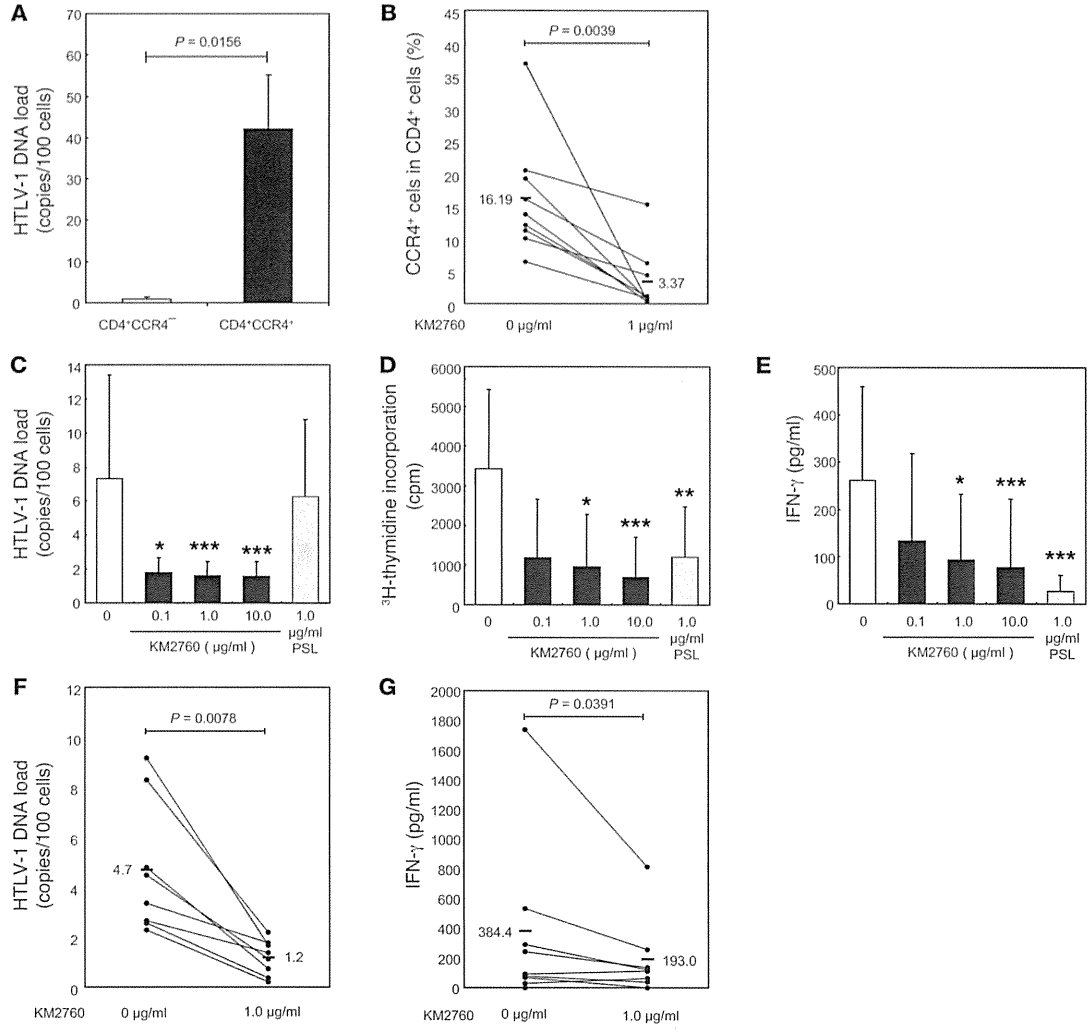

Figure 5. CCR4 shows potential as a molecular target for HAM/TSP immunotherapy. (**A**–**G**) Cells isolated from HAM/TSP patients were sorted via FACS (**A**; $n = 7$) or cultured for 7 days under the following conditions: PBMCs were cultured with various concentrations of KM2760 or 1 μg/ml PSL (**B**–**E**; $n = 9$), and CSF cells were cultured with 1 μg/ml KM2760 (**F** and **G**; $n = 8$). (**A**, **C**, and **F**) HTLV-1 proviral DNA loads were measured using quantitative PCR. (**D**) Degree of spontaneous proliferation was assessed by measuring ^{3}H-thymidine incorporation. (**E** and **G**) IFN-γ production in the culture media was evaluated using CBA assays. HTLV-1 resided in $CD4^+CCR4^+$ rather than $CCR4^-$ cells among PBMCs (**A**), and KM2760 treatment effectively targeted these cells (**B**). Consequently, KM2760 treatment successfully reduced HTLV-1 proviral DNA load (**C**), suppressed spontaneous proliferation (**D**), and decreased IFN-γ production (**E**) in PBMC cultures as well as reducing HTLV-1 DNA load (**F**) and IFN-γ production (**G**) in CSF cell cultures derived from HAM/TSP patients. (**A** and **C**–**E**) Data are mean ± SD. (**B**, **F**, and **G**) Thick horizontal bars represent mean value for all patients; line segments represent individual patients. Statistical analyses were performed using Friedman test followed by Dunn test for multiple comparisons (**C**–**E**) or Wilcoxon test (**A**, **B**, **F**, and **G**). $^*P < 0.05$, $^{**}P < 0.01$, $^{***}P < 0.001$ vs. untreated control.

sion profile (19). We suspected that these infected cells may infiltrate the CNS and trigger an inflammatory positive feedback loop, ultimately leading to chronic spinal cord inflammation (27). In the present study, we provided concrete evidence to support these theories on HAM/TSP pathogenesis, with a particular emphasis on the mechanism by which Tax can induce a proinflammatory phenotype intracellularly via transcriptional regulation.

There is strong evidence to support the conclusion that a substantial portion of the Treg population in HAM/TSP patients is infected with HTLV-1 (28, 29). In a previous study, we demonstrated that $CD4^+CD25^+CCR4^+$ cells were the main reservoir for HTLV-1 in HAM/TSP patients (19), but that expression profile is not exclusive to Tregs. Our present observation that $CD4^+$ T cells positive for FOXP3, a well-established marker for Tregs (10), were more thoroughly infected than the $GATA3^+$ subgroup (Figure 1A) strengthens the argument that Tregs may be the main viral reservoir. It remains debatable whether the virus preferentially infects these cells, promotes their survival (30), or even induces the expression of these

markers. One report postulates that HTLV-1 preferentially infects $CCR4^+$ cells by upregulating CCL22 to encourage cell-to-cell transfer via chemotactic attraction (31). More research is necessary to determine the true mechanism by which infected $CCR4^+$ and $FOXP3^+$ cells become so abundant in HAM/TSP patients.

We demonstrated that the suppressive ability of $CD4^+CD25^+$ $CCR4^+$ cells that characterizes Treg function was impaired by expression of the Tax protein, encoded in the pX region of the HTLV-1 genome (Figure 1B). Prior evidence indicates that Tax may exert these effects via downregulation of FOXP3 expression (20, 32). Transgenic mice expressing Tax exhibit reduced $CD4^+CD25^+FOXP3^+$ Tregs (33) and develop arthritis (34), and transgenic rats expressing HTLV-1 env-pX develop destructive arthropathies, Sjogren syndrome, vasculitis, and polymyositis (35). Collectively, these observations suggest that Tax expression can lead to inflammatory disease by weakening immune tolerance and disrupting homeostasis.

It has long been suspected that in addition to reducing FOXP3 expression, Tax may have the ability to induce IFN-γ production, thereby converting once-suppressive cells into proinflammatory cells. Indeed, intracellular Tax expression has been associated with the rapid upregulation of IFN-γ in infected cells, and researchers have theorized that this upregulation may contribute to the pathogenesis of HTLV-1–associated inflammatory disorders, including HAM/TSP (19, 36, 37). Here we showed at the mRNA level that *Tax* expression stimulated *IFNG* expression; moreover, the effect appeared delayed (Figure 2A), in a manner suggestive of 1 or more intermediate steps in the pathway, rather than direct transcriptional activation. Several candidate pathways have been proposed— such as via NF-κB, STAT1, or STAT5 — but none have been confirmed experimentally (38, 39).

We provided convincing evidence that Tax induces IFN-γ production in infected cells indirectly by amplifying the effects of Sp1 binding to — and increasing the activity of — the *TBX21* promoter: the resulting amplification of T-bet expression was responsible for the rise in IFN-γ production.

T-bet is said to be a Th1-specific T box transcription factor that controls the expression of the hallmark Th1 cytokine, IFN-γ (6). *TBX21*-deficient mice exhibit greater resistance to a variety of inflammatory and autoimmune diseases than their wild-type counterparts (40). Thus, it has been of interest that elevated *TBX21* levels have been found in the PBMCs of HAM/TSP patients (41). We showed that *TBX21* expression was elevated in the $CD4^+CD25^+CCR4^+$ cells of HAM/TSP patients, but not ATLL patients (Figure 2B and Supplemental Figure 1), which suggests that this trait is specific to HAM/TSP pathogenesis. Furthermore, we interpreted the lack of elevation in $CD4^+CD25^-CCR4^-$ cells to indicate that elevated *TBX21* is characteristic of infected cells. Importantly, we clearly demonstrated for the first time that Tax induced T-bet expression (Figure 2, C and E, and Supplemental Figures 2 and 3). Moreover, we showed that this pathway was active in $CD4^+CD25^+CCR4^+$ cells of HAM/TSP patients by silencing Tax expression and observed a corresponding reduction in *TBX21* expression; in the reverse scenario, inducing Tax expression in otherwise-normal $CD4^+CD25^+CCR4^+$ cells from HDs resulted in heightened *TBX21* expression (Figure 2D and Supplemental Figure 2). Finally, we confirmed that this correlation extended to protein production and clearly showed how Tax induces T-bet and subsequently IFN-γ production over time in culture (Figure 2E).

Tax has been reported to stably bind Sp1, a known positive transcriptional regulator of *TBX21* (25, 42). More specifically, interaction with Tax is thought to increase the DNA binding activity of Sp1 (42). Here we used co-IP with samples from the HTLV-1–infected MT-2 cell line to show that endogenous Tax interacted with Sp1 (Figure 3A). Subsequently, ChIP assays revealed that both Sp1 and Tax associated with the *TBX21* promoter region (Figure 3B), a novel finding that supports our theory that Tax and Sp1 together activate *TBX21* transcription. Finally, we showed that in the absence of Sp1, Tax had no significant effect on *TBX21* expression; however, in the presence of Sp1, Tax induced *TBX21* expression in a concentration-dependent manner (Figure 3C). This finding further substantiates our claim that Tax does not directly bind the promoter, but rather acts via Sp1. It should be noted that Tax may induce *TBX21* expression via multiple pathways: it has been reported that Tax enhances STAT1 gene expression in HTLV-1–transformed T cell lines and $CdCl_2$-stimulated JPX-9 cells (38), which suggests that Tax may also induce *TBX21* expression indirectly via STAT1.

The presence of T cell infiltrates in the CNS, indicative of spinal cord inflammation, is a well-known feature of HAM/TSP. Researchers have worked to characterize these cells over the years; together, their findings suggest that the infiltrates are dominated by $CD4^+$ T cells with relatively high proviral loads and elevated Tax and IFN-γ expression (43–45). We hypothesized that a substantial portion of the infiltrate may be made up of infected $CD4^+CCR4^+$ T cells exhibiting Th1-like properties, including IFN-γ production. We used immunohistochemistry to investigate this theory and were able to establish the presence of $CD4^+CCR4^+CXCR3^+$T-$bet^+IFN\text{-}\gamma^+$ cells in spinal cord tissue and HTLV-1–infected $CCR4^+$ cells in the CSF of HAM/TSP patients (Figure 4, A and B). We used FACS analysis to confirm that $CD4^+CCR4^+CXCR3^+$ cells made up the majority of the $CD4^+$ T cells in the HAM/TSP patient CSF (Figure 4C). For the sake of continuity between this and our previous study (19), we also confirmed that the majority of these $CD4^+CCR4^+CXCR3^+$cellswerealso$CD25^+$(SupplementalFigure5), further suggestive of a Treg identity.

We interpret the observation that these $CD4^+CCR4^+CXCR3^+$ cells were virtually nonexistent among PBMCs in HAM/TSP patients (Figure 4D) to mean that the cells had migrated to the CNS, leaving few behind in the periphery. The surprising observation that the Ki67 marker for cell proliferation was negative in the overwhelming majority of $CD4^+CCR4^+CXCR3^+$ cells in the CSF (Figure 4E) signifies that the cells are indeed proliferating elsewhere and subsequently migrating to the CNS. It has in fact been said that HTLV-1–infected cells may be extraordinarily capable of crossing the blood-brain barrier (46). Due to the high proportion of CCR4 positivity among HTLV-1–infected cells (19), the high proviral load in the CSF of HAM/TSP patients (47), and the elevated levels of CCL22 in HAM/TSP patient peripheral blood (30), one might hypothesize that the infected cells migrate across the blood-brain barrier in response to chemokine ligands of CCR4, namely CCL22. However, we found that the CSF of HAM/TSP patients contained only negligible amounts of CCL22, instead favoring the CXCR3 ligand CXCL10 (48). We now postulate that

$CD4^+CCR4^+CXCR3^+$ T cells and other $CXCR3^+$ cells may migrate to the CNS via chemotaxis induced by CXCL10 secreted by astrocytes in the CNS. Previously, we showed that these astrocytes produce CXCL10 in response to IFN-γ, and these levels are further amplified by the invading $CXCR3^+$ cells (27). Together, these findings indicate that a positive feedback loop involving the recruitment of proinflammatory cells to the CNS is the source of chronic inflammation in HAM/TSP, and that the original trigger is the migration of IFN-γ–producing HTLV-1–infected cells to the CNS. Where these proinflammatory cells are primarily proliferating, and why they proliferate at different rates in different settings, are questions to be addressed in future studies.

Our findings in this and previous studies imply that targeting $CCR4^+$ cells could constitute an effective treatment for HAM/TSP. Indeed, this strategy is already in play for ATLL patients, the majority of whom suffer from $CCR4^+$ T cell–derived cancers (7). The humanized defucosylated anti-CCR4 monoclonal antibody KW-0761, which has been shown to induce CCR4-specific ADCC, has been approved as a treatment for ATLL (49, 50). The observation that the majority of infected $CD4^+$ PBMCs in HAM/TSP patients were $CCR4^+$ (Figure 5A) suggests that an anti-CCR4 antibody with ADCC properties might be used to effectively treat HAM/TSP patients as well. Steroids are currently the standard of care for HAM/TSP patients, but this approach is not considered optimal: as with many nonspecific treatments, the effectiveness is limited, and the side effects are numerous (51). Here we compared the effects of the defucosylated chimeric anti-CCR4 monoclonal antibody KM2760 (21) with those of the steroid PSL on ex vivo cultures of cells from HAM/TSP patients. Although PSL had more potent effects per microgram, both treatments successfully reduced cell proliferation and IFN-γ production (Figure 5, D, E, and G). In addition, even a small dose of the antibody effectively reduced proviral load, whereas PSL treatment had no significant effect (Figure 5, C and F). These findings support the main premise of this paper, namely, that $CCR4^+$ cells are major viral reservoirs and producers of IFN-γ. Our study is the first to test the effects of such an antibody-based treatment on cells from HAM/TSP patients; the results were promising, and a clinical trial investigating the in vivo effectiveness in HAM/TSP patients is now underway. Importantly, our research indicates that even if the antibody does not cross the blood-brain barrier, it could be therapeutically effective against spinal cord inflammation by eliminating the proinflammatory $CCR4^+$ cells in the peripheral blood that would have migrated to the CNS.

Until very recently, there had been no reports of T cell character changing from suppressive to inflammatory in response to internal transcriptional alterations induced intracellularly by viral products. There have been many reports of Tregs transforming in the presence of inflammation due to the influence of cytokines, including instances where FOXP3 expression is lost and even cases where IFN-γ production is gained (12, 13). The only report of a similar phenomenon occurring via an intracellular virus-induced pathway states that the HTLV-1 basic leucine zipper (HBZ) gene product can reduce the expression of FOXP3 in HBZ-transgenic mouse Tregs (52). Here we showed for the first time that the HTLV-1 virus can similarly affect gene expression in human cells, inducing IFN-γ production, as well as reduce suppressive function. Collectively, the research to date suggests that HTLV-1 may preferentially infect $CCR4^+$ cells, including Tregs, and induce transcriptional changes via Tax that not only reduce FOXP3 expression, but also induce T-bet expression and consequently IFN-γ production, yielding a proinflammatory immune imbalance. While there is considerable evidence to support this theory, further experiments are necessary to prove that this pathway is indeed the origin of HAM/TSP chronic inflammation. However, here we have directly shown that the HTLV-1 protein product Tax can induce the expression of the Th1 master transcription factor T-bet, which certainly implies that HTLV-1 is capable of activating inherent plasticity in T cells and shifting their gene expression profiles toward a Th1-like state.

Methods

Patient selection and sample preparation. The study included HTLV-1–noninfected HDs ($n = 8$, 4 male and 4 female; mean age, 36 yr), asymptomatic carriers ($n = 6$, 4 male and 2 female; mean age, 56 yr), ATLL patients ($n = 6$, 2 male and 4 female; mean age, 68 yr), and HAM/TSP patients ($n = 31$, 9 male and 22 female; mean age, 61 yr). Diagnosis of ATLL was based on the criteria established by Shimoyama (53). HTLV-1 seropositivity was determined by a particle agglutination assay (Serodia-HTLV-1) and confirmed by Western blot (SRL Inc.). HAM/TSP was diagnosed according to WHO guidelines (54).

Samples of PBMCs were prepared using density gradient centrifugation (Pancoll; PAN-Biotech) and viably cryopreserved in liquid nitrogen (Cell Banker 1; Mitsubishi Chemical Medience Corp.). CSF samples were taken from 17 HAM/TSP patients. CSF cells were isolated by centrifugation and cryopreserved in the aforementioned freezing medium until use. Thoracic spinal cord tissue samples from 1 HAM/TSP patient were obtained postmortem, fixed in 10% formalin, and embedded in paraffin.

Antibodies. For FACS studies, labeled anti-CD3 (UCHT1), anti-CD4 (OKT4), anti-GATA3 (TWAJ), and anti-FOXP3 (PCH101) were purchased from eBioscience, and labeled anti-CCR4 (1G1), anti-CD25 (BC96), anti-CXCR3 (1C6), anti–T-bet (4B10), and anti-Ki67 (B56) were purchased from BD Biosciences. For IP studies, anti-Sp1 (PEP2) and normal IgG were purchased from Santa Cruz Biotechnology Inc., and anti-Tax (Lt-4) was prepared as described previously (55). For immunofluorescence studies, anti-CCR4, anti–IFN-γ, and anti-CXCR3 were purchased from Abcam; anti–T-bet was purchased from Santa Cruz Biotechnology Inc.; and Alexa Fluor 488– and Alexa Fluor 594–conjugated secondary antibodies were purchased from Invitrogen. Kyowa Hakko Kirin Co. Ltd. provided KM2760, a chimeric anti-CCR4 IgG1 monoclonal antibody (21).

Plasmids. The *TBX21*-Luc reporter gene plasmid was constructed as described previously (25). The 100-bp promoter fragment (–101 to –1) in the 5′-flanking region of the human *TBX21* gene was obtained by PCR using human PBMC genomic DNA as the template. Primers used for PCR were 5′-CGCCTCGAGGGCGGGGTGGGGCGAGGCGG-3′ and 5′-CCCAAGCTTCTGTCACTAGAGTCGCAGCGCTTT-3′. The amplified PCR product was digested with XhoI/HindIII and cloned into pPicaGene-Basic vector II (Toyo-ink), which yielded *TBX21*-Luc. Creation of the human Sp1 construct with HA-tag added to the N terminus was accomplished via real-time RT-PCR amplification of human PBMC cDNA with the following primers: Sp1 forward, 5′-CGCGAATTCATGAGCGACCAAGATCACTCCATGGA-3′; Sp1 reverse, 5′-CGCCTCGAGTCAGAAGCCATTGCCACTGATATTAATGGAC-3′. The amplified fragment was digested with EcoRI/XhoI and

subcloned into HA-tagged pcDNA3 (Invitrogen). Tax construct with FLAG-tag added to the N terminus was prepared via PCR amplification of template DNA (56) with the following primers: Tax forward, 5′-CGCGAATTCATGGCCCACTTCCCAGGGTTT-3′; Tax reverse, 5′-CGCCTCGAGTCAGACTTCTGTTTCACGGAAATGTTTTTC-3′. The amplified fragment was digested with EcoRI/XhoI and subcloned into FLAG-tagged pcDNA3. The plasmid HTLV-1 provirus (pUC/HTLV-1) was provided by T. Watanabe (University of Tokyo, Tokyo, Japan) (57). A lentiviral vector, CSIICMV, was used as a null expression vector for lentiviral infection (provided by H. Miyoshi, RIKEN BioResource Center, Tsukuba, Japan) (58). CSIICMV/GFP and CSIICMV/GFP-Tax, which express GFP and GFP fused Tax, were constructed by inserting digested GFP and GFP-Tax from pEGFP (Clontech) and pEGFP-Tax, respectively, into CSIICMV.

Flow cytometric analysis. PBMCs and CSF cells were immunostained with various combinations of the following fluorescence-conjugated antibodies that tag cell surface markers: CD3 (UCHT1), CD4 (OKT4), CD25 (BC96), CCR4 (1G1), CXCR3 (1C6). In some experiments, cells were fixed with a staining buffer set (eBioscience), then intracellularly stained with antibodies against T-bet (4B10), FOXP3 (PCH101), and GATA3 (TWAJ). Cells were stained with a saturating concentration of antibody in the dark (4°C, 30 minutes) and washed twice before analysis using FACSCalibur or LSR II (BD Biosciences). Data were processed using FlowJo software (TreeStar). For cell sorting, JSAN (Bay Bioscience) was used, and the purity exceeded 95%.

Cell isolation. $CD4^+CD25^+CCR4^+$ cells, $CD4^+CD25^-CCR4^-$ cells, $CD4^+GATA3^+$ cells, and $CD4^+FOXP3^+$ cells were separated by FACS sorting. $CD4^+$ T cells were isolated from PBMCs using negative selection with magnetic beads (MACS $CD4^+$ T cell isolation kit; Miltenyi Biotec). $CD4^+CCR4^-$ or $CD4^+CCR4^+$ cells were then isolated from these $CD4^+$ T cells using positive selection with anti-CCR4 Ab (1G1) and rat anti-mouse IgG1 microbeads (Miltenyi Biotec).

Cell culture conditions. HEK293 cells were cultured in MEM (Wako Pure Chemical Industries) supplemented with 10% heat-inactivated FBS (Gibco, Invitrogen) and 1% penicillin/streptomycin (P/S) (Wako Pure Chemical Industries). HEK293T cells were cultured in DMEM-high glucose (Sigma-Aldrich) supplemented with 10% FBS and 1% P/S. Jurkat, MT-2, and JPX-9 cells were cultured in RPMI 1640 medium (Wako Pure Chemical Industries) supplemented with 10% FBS and 1% P/S. JPX-9 is a subline of Jurkat carrying Tax under the control of the metallothionein promoter (provided by M. Nakamura, Tokyo Medical and Dental University, Tokyo, Japan) (59), by which Tax expression is inducible by the addition of 20 μM $CdCl_2$ (Nacalai Tesque Inc.). PBMCs, $CD4^+CCR4^+$ cells, $CD4^+CD25^+CCR4^+$ cells, and $CD4^+CD25^-CCR4^-$ cells isolated from HDs or HAM/TSP patients were cultured in RPMI 1640 medium supplemented with 5% human AB serum (Gibco, Invitrogen) and 1% P/S.

Gene expression profiling and analyses. For transcriptional profiling, $CD4^+CD25^+CCR4^+$ T cells from a HAM/TSP patient, an ATLL patient, and an HD were separated using FACS sorting. Total RNA was prepared using ISOGEN (Nippon gene) following the manufacturer's recommendations. RNA was amplified and labeled with cyanine 3 (Cy3) using an Agilent Quick Amp Labeling Kit, 1-color (Agilent Technologies), following the manufacturer's instructions. For each hybridization, Cy3-labeled cRNA were fragmented and hybridized to an Agilent Human GE 4x44K Microarray (design ID 014850). After washing, microarrays were scanned using an Agilent DNA microarray scanner. Intensity values of each scanned feature were quantified using Agilent feature extraction software (version 9.5.3.1), which performs background subtractions. All data were analyzed using GeneSpring GX software (Agilent Technologies). There were a total of 41,000 probes on Agilent Human GE 4x44K Microarray (design ID 014850), not including control probes. Microarray data were deposited in GEO (accession no. GSE57259).

Real-time PCR and real-time RT-PCR. The HTLV-1 proviral DNA load was measured using ABI Prism 7500 SDS (Applied Biosystems) as described previously (19). For real-time RT-PCR analysis, total RNA isolation and cDNA synthesis were performed as described previously (19). Real-time PCR reactions were carried out using TaqMan Universal Master Mix (Applied Biosystems) and Universal Probe Library assays designed using ProbeFinder software (Roche Applied Science). ABI Prism 7500 SDS was programmed to have an initial step of 2 minutes at 50°C and 10 minutes at 95°C, followed by 45 cycles of 15 seconds at 95°C and 1 minute at 60°C. The primers used were as follows: *TBX21*, 5′-TGTGGTCCAAGTTTAATCAGCA-3′ (forward) and 5′-TGACAGGAATGGGAACATCC-3′ (reverse) (probe no. 9; Roche Applied Science); *Tax*, 5′-ATACAACCCCCAACATTCCA-3′ (forward) and 5′-TTTCGGAAGGGGGAGTATTT-3′ (reverse) (probe no. 69; Roche Applied Science). The primers and probes for detecting *Tax*, *IFNG*, and *GAPDH* mRNA were described previously (19). Relative quantification of mRNA was performed using the comparative Ct method using GAPDH as an endogenous control. For each sample, target gene expression was normalized to the expression of GAPDH, calculated as $2^{-(Ct[target]-Ct[GAPDH])}$.

Virus preparation and cell infection. 293T cells (1×10^6) plated in 100-mm dishes were cotransfected with the appropriate lentiviral-GFP or lentiviral-GFP-Tax expression vector (17 μg), vesicular stomatitis virus G expression vector VSV-G (pMD.G) (5 μg), rev expression vector pRSVRev (5 μg), and gag-pol expression vector pMDLg/pRRE (12 μg) (60) using Lipofectamine 2000 (Invitrogen) according to the manufacturer's protocol. After 4 hours, cells were washed 3 times with PBS, 5 ml of new medium was added, and cells were incubated for 48 hours. Culture supernatants were harvested and filtered through 0.45-μm pore size filters. Lentivirus was concentrated approximately 40-fold by low centrifugation at 6,000 *g* for 16 hours and resuspended in 2 ml RPMI 1640 medium. Freshly isolated $CD4^+CD25^+CCR4^+$ T cells were activated using Treg Suppression Inspector (Anti-Biotin MACSiBead Particles preloaded with biotinylated CD2, CD3, and CD28 antibodies) according to the manufacturer's protocol (Miltenyi Biotec). After being cultured for 36 hours, cells were transduced with equal amounts of the GFP or GFP-Tax lentivirus (MOI 15), followed by centrifugation for 1 hour at 780 *g*, 32°C. After being cultured for 4 hours at 32°C, cells were washed with culture medium and cultured in round-bottomed 96-well plates at 37°C.

Treg suppression assay. A study was conducted to compare the capacities of GFP versus GFP-Tax lentivirus–infected $CD4^+CD25^+CCR4^+$ T cells to suppress cell proliferation. T cell samples were taken from HDs, and 5×10^4 $CD4^+CD25^-$ T cells were stimulated with the Treg Suppression Inspector (see above) according to the manufacturer's instructions. These cells were then cocultured with 5×10^4 GFP lentivirus–infected $CD4^+CD25^+CCR4^+$ T cells or GFP-Tax lentivirus–infected $CD4^+CD25^+CCR4^+$ T cells. After culturing for 4 days, cell proliferation was measured using a ^3H-thymidine incorporation assay as described previously (19).